Sulphur-reduced graphene oxide composite with improved electrochemical performance for supercapacitor applications

Delvina Japhet Tarimo, Kabir O. Oyedotun, Abdulmajid A. Mirghni and Ncholu Manyala*.

Department of Physics, Institute of Applied Materials, SARChI Chair in Carbon Technology and Materials, University of Pretoria, Pretoria 0028, South Africa.

*Corresponding author's email: ncholu.manyala@up.ac.za, Tel.: + (27)12 420 3549.

HIGHLIGHTS

- RGO-S was synthesized by a modified Hummers method.
- Combination of nanosheet, nanorods and nanofibers morphologies were observed.
- High specific capacity of about 113.8 mAh g^{-1} was recorded for the half cell.
- The material displayed specific energy and power of 35.2 Wh kg^{-1} and 375 W kg^{-1} at 0.5 Ag^{-1}, respectively.
- The fabricated material revealed good electrochemical performance for future supercapacitor applications.

ABSTRACT

In this research, carbon nanorods/fibers material were successfully synthesized from sulphur-doped reduced graphene oxide (RGO-S) by using an improved Hummers method. Morphological, structural, compositional and textural characterization of the composite material were obtained via scanning electron microscope (SEM), energy dispersive x-ray spectroscopy (EDX), transmission electron microscopy (TEM), X-ray diffraction (XRD), Raman spectroscopy, Fourier transform infrared spectroscopy (FTIR) and X-ray photoelectron spectroscopy (XPS), respectively. The electrochemical performance of the composite sample as a promising supercapacitor electrode revealed a peak specific capacity of 113.8 mAh g^{-1} at 0.5 A g^{-1} estimated via GCD curves in 6 M KOH aqueous electrolyte. The half-cell could retain a columbic efficiency of about 98.7 % with a corresponding energy efficiency of about 98.5 % over 2,000 constant charge/discharge cycle at a specific current of 5 A g^{-1}. Remarkably, an assembled hybrid device with carbonized iron cations

(C-FP) and the RGO-S composite delivered high energy and power densities of 35.2 Wh kg^{-1} and 375 W kg^{-1} at 0.5 A g^{-1} within a 1.5 V operating potential, respectively. A good cycling stability performance with an energy efficiency of 99 % was observed for the device for up to 10,000 cycling at a specific current of 3 A g^{-1}.

GRAPHICAL ABSTRACT

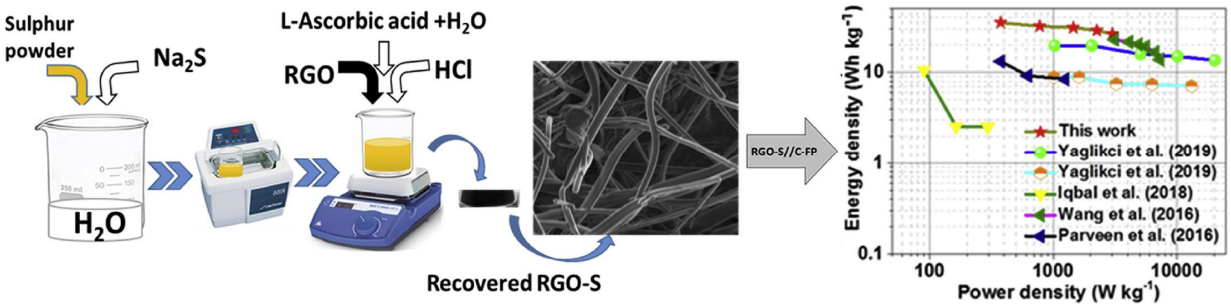

KEYWORDS: Carbon nanorods/fibers, sulphur-doped reduced graphene oxide (RGO-S), carbonized iron cations (C-FP), energy density, capacity retention.

1. INTRODUCTION

Sufficient resources of energy and their adequate effective usage are some major factors crucial to the growth of our socio-economical modern civilizations. The reliability on the fossil fuel as a main source of energy is heading to an extinction. In the light of this, there is an urgent call to source for alternative sources of energy. This challenge remains critical in our everyday life and thus, requires urgent solutions [1,2]. In order to address this problem, practicable energy storage technology is required to proffer solutions to the lingering energy problem for immediate future demand.

Due to massive effect caused by climatic change and high consumption of fossil fuels, there has been a great interest in developing alternative improved energy storage systems. Such systems include supercapacitors, batteries and other energy conversion system like fuel cells and solar cells [3–8]. Supercapacitor, a device that stores charges by electrochemical process has been considered a potential candidate for efficient energy storage due to its excellent cycling stability, high power density and fast charge/discharge ability [9,10].

Supercapacitors can be categorized into three types: I. Electric double-layer capacitor (EDLCs) which mechanism of charging/discharging is based on the electrostatic process whereby energy is stored by adsorption of ions on the surface of the electrode. II. Redox capacitor which employs faradic mechanism occurring on the surface of the electrode that involves charge-transfer from redox reactions. In redox capacitor the faradic phenomenon involves fast and reversible electrochemical reactions between the electrolyte and electrode materials. III. Hybrid supercapacitor combines faradic electrode material and EDLCs to make up hybrid system [4,10–12].

Normally, carbon based materials such as activated carbon, carbon fibres, graphene, conducting polymers and metal oxides has been categorized as some of the materials used for fabrications of supercapacitors [6,13,14]. However, conducting polymers and transition metal oxide has been faced with low charge discharge rate and cycling stability [15–18].

Graphene has attracted researchers' interest due to its worthy mechanical and chemical stability, high electrical conductivity, larger specific surface area and low cost [3,9,19]. In spite of these excellent properties of the material, when the graphene as electrode material employed in an energy storage devices such as supercapacitors, it is still plagued with low specific capacitance [4,14]. Thus modification of its surface chemistry such as by optimizing the oxygen-containing surface functionalities, as well as morphological properties can improve electrochemical

performance of the material [3,8,18–20]. Besides, the introduction of heteroatoms such as sulphur (S), nitrogen (N), boron (B) and phosphorus (P) had been seen to improve the electrochemical performance of the material. Integration of heteroatom into carbon materials has improved electrical and surface properties, decreased charge transfer resistance and improved wettability of graphene-related materials [5,7,11,21].

Incorporation of these heteroatoms by either substitutions or replacement into graphene materials creates defects into graphene as a result of changes in the graphene properties [19,22]. Graphene doped with sulphur is of specific interest due to charge transfer in C-S bond arising from the slight difference in electronegativity of S (2.58) and carbon (2.55) [7,23,24]. Also, sulphur can be easily polarized, thus increase chemical reactivity of the graphene. Yaglikci et al. reported on sulphur doped activated carbon prepared using microwave and activation at 850 ^{o}C and obtained a smaller pitted shapes with energy and power densities of 20.1 Wh kg^{-1} and 294.35 W kg^{-1} respectively, at 1 A g^{-1} in 6M KOH electrolyte and, energy and power densities of 9.06 Wh kg^{-1} and 400.10 W kg^{-1} respectively, at 1 A g^{-1} in 1M H_2SO_4 electrolyte [6]. Nitrogen and sulfur co-doped carbon nanosheets derived from willow catkin reported by Wang et al. was prepared by pyrolisis and activation at 850 ^{o}C displayed interconnected carbon nanosheets with energy and power densities of 21 Wh kg^{-1} and 180 W kg^{-1} respectively, at 50 A g^{-1} in 1M Na_2SO_4 electrolyte [11]. Iqbal et al. prepared graphene oxide based strontium sulfide using hydrothermal method and obtain nanorods like morphology with few bunches indicating an incomplete growth of nanorods that exhibited energy and power densities of 10.55 Wh kg^{-1} and 294.35 Wh kg^{-1} respectively, at 0.5 $mAcm^{-2}$ in 2M KOH electrolyte [13]. Parveen et al. obtained sulfur doped graphene using electrochemical exfoliation method and obtained a transparent sheets with a small black dots with energy density of 9.6 Wh kg^{-1} and power density of 375.7 Wh kg^{-1} at 5 A g^{-1} in 3M KOH electrolyte [25]. These results show that heteroatom doped carbon materials demonstrated synergetic electrochemical properties due to high electron donating property and charge density enhancement of carbon

materials. However, in most cases chemical and thermal treatment were used to prepare carbon based doped material in which it requires high energy, longer reaction time and organic solvents in order to reduce functional groups in graphene oxide which become problems for mass production [7].

In this study, we report on the role of morphology control through the addition of sulphur in enhancing electrochemical performances of graphene-based supercapacitors via an environmentally friendly and cost-effective synthesis method. The synthesized material was obtained from sulphur-doped reduced graphene oxide (RGO-S) by using an improved Hummers method. The as-synthesized electrode was characterized by different techniques and the electrochemical performance was evaluated in both three and two-electrode systems using 6 M KOH electrolyte. In a three-electrode setup, the fabricated materials displayed a highest specific capacity of 113.8 mAh g^{-1} at 0.5 A g^{-1} evaluated from the galvanostatic charge-discharge (GCD) curve. Remarkably, an assembled hybrid device with carbonized iron cations (C-FP) and the RGO-S composite delivered high energy and power densities of 35.2 Wh kg^{-1} and 375 W kg^{-1} at 0.5 A g^{-1} at an operating potential of 1.5 V, respectively. The as-synthesized material revealed good electrochemical properties, which proves its promising potential as electrode material for supercapacitor applications.

2. EXPERIMENTAL DETAILS

2.1 Preparation of Reduced Graphene Oxide (RGO) Samples

Graphene oxide was prepared by a modified hummer's method using graphite powder [4,14,26]. Graphite powder (5 g) was added slowly to 100 mL of sulphuric acid (H_2SO_4) which serve as an intercalated molecules for the penetrating oxidation of bulk graphite in an ice bath to cool the acid. Thereafter, 2.5 g each of potassium hydrogen sulphate ($KHSO_4$) and calcium chloride ($CaCl_2$)

were added subsequently upon stirring. $KHSO_4$ was used to start up the reaction while $CaCl_2$ used as a water remover. Effervescence was noticed upon additional of $CaCl_2$. The resulting mixture was stirred (400 rev/min) for 40 min. at 60 ^oC, followed by a further addition of 10 g of potassium permanganate ($KMnO_4$) as an oxidizing agent and additional 50 mL of H_2SO_4. The solution was further stirred (250 rev/min) for 2 hours at 60 ^oC for homogeneity. The dark-grey resulting mixture was removed from the heating plate and left to cool down to room temperature. Thereafter, 20 mL of hydrogen peroxide (H_2O_2 - 30 %) alongside 120 mL of deionized water (DI water) were added to stop the reaction, which caused a vigorous rise in temperature of the mixture and beard great potential hazard. Therefore, great caution must be taken during the synthesis of the material. The resulting mixture called graphene oxide (GO) was allowed to cool down naturally to room temperature, and thereafter was re-dispersed into a 100 mL of DI water and sonicated for 2 hours for further reduction of GO. Sonication uses sound energy to agitate atoms in a solution whereby it converts an electrical signal into a physical vibration to break materials apart. These disturbances can mix solutions, accelerate the dissolution of GO into a liquid and remove dissolved gas from liquids. The mixture was left to settle down for 12 hours, washed several times with DI water and then centrifuge and dried in a vacuum oven at 80 ^oC for 6 hours to obtain the final sample named as reduced graphene oxide (RGO).

2.2 Preparation of Sulphur-doped Reduced Graphene Oxide (RGO-S) Composite

1 g of sulphur powder together with 3 g of sodium sulphide (Na_2S) act as a sulphur source were added into 100 mL of DI water and sonicated until a homogenous solution named ‘A’ was formed. 50 g of L-Ascorbic acid used a reducing agent was liquefied in 12 g of DI water to form a solution named ‘B’. Thereafter, 3 g of as-synthesized RGO was mixed into solution ‘A’ together with solution ‘B’ and the resulting mixture was named as solution ‘C’. Subsequently, 2 mL of HCl was added to the mixture (solution ‘C’) and then stirred for 5 min. The little volume of HCl added to

the mixture was not to cause a further reaction, but to alter the pH of the mixture as well as for the purpose of ion exchange, which resulted in effective polarity. Besides, H_2S that may be formed in the addition of the HCl is soluble in water and was not expected to be part of the sulphur in the rGO matrix. The mixture was sonicated for 2 h and then stirred (400 rev/min.) for 1 h at 40 ^oC, centrifuged for 10 min. at 5000 rpm and dried at 80 ^oC for 12 hours in a vacuum oven. The as-synthesized sample was named as sulphur doped reduced graphene oxide (RGO-S).

2.3 Preparation of polyaniline (PANI)

The PANI material employed in this study was synthesized as described in our previous publication [27]. In brief, 0.2 M aniline hydrochloride was added to 0.25 M of ammonium peroxydisulfate. The mixture was stirred for 10 minutes, and then left to stand overnight for polymerization. The supernatant was decanted away and the recovered precipitate was washed several times with deionized. The resulting sample was dried overnight in an electric oven at 60 ^oC under ambient condition.

2.4 Preparation of Carbonized Iron Cations Adsorbed onto PANI (C-FP) Material

0.4 g iron (II) nitrate nonahydrate, 0.5 g of polyaniline (PANI), 0.25 g each of polyvinylidene fluoride (PVDF) and carbon acetylene black (CAB) were mixed together and then completely dispersed into 20 mL of 99.9 % ethanol. PVDF was used as a binder to bind the material onto nickel foam while CAB was added as a conducting agent. The mixture was sonicated until it evaporated to slurry. The slurry was coated into nickel foam and then annealed at a ramping rate of 17 °C/min until 850 °C in nitrogen (500 cc flow rate) gas environment at a dwell time of 2 h to obtain iron cations (Fe^{2+}) adsorbed onto the PANI film (C-FP) directly grown onto the nickel foam. At this temperature of 850 °C, the PANI film decomposed into the nickel foam template on which the material was coated. The precursors' masses were carefully selected to ensure an approximate weight ratio of 80:10:10 for iron (II) nitrate salt and PANI, CB and PVDF respectively [27].

2.5 Characterization of the Samples

The transmission electron microscope (TEM) and scanning electron microscope (SEM) equipped with an energy-dispersive X-ray (EDX) of the as-synthesized samples were obtained from a JEOL-2100F high resolution transmission electron microscope (HRTEM FEI Tecnai-F30) alongside 200kV acceleration voltage and a Zeiss Ultra Plus 55 field emission scanning electron microscope (FE-SEM) operated at 1.0 kV and 2.0 kV, respectively. The material's phase structure was analyzed by a Bruker BV 2D PHASER Best Benchtop X-ray diffraction (XRD) analyzer with reflection geometry at 2θ values (5–90°) with a step size of 0.005 °, operating with a Cu $K\alpha_1$ radiation source (λ = 0.15406 nm) at 50 kV and 30 mA. A WITec alpha 300 RAS+ Confocal micro-Raman microscope operated at 532 nm laser wavelength was used to characterize the as-prepared sample with a spectral acquisition time of 150 s and laser power of 5 mW on the sample to avoid sample heating. Fourier transform-infrared (FTIR) analysis was achieved via a Varian FT-IR spectroscopy in a range of 500 – 4000 cm^{-1} in wavenumber. An X-ray photoelectron spectroscopy (XPS) analyzer (Versa Probe 5000 spectrometer activated with a 100 μm monochromatic Al-Kα exciting source) was employed to analyze the electronic states of surface elements present in the composite sample.

2.6 Electrochemical Characterization

The three- and two-electrode systems were used to carry out the electrochemical measurements. For the three-electrode system, the working electrode was prepared by mixing 80 % of the active material with 10 % each of conductive carbon acetylene black (CB) and Polyvinylidene fluoride (PVDF) as a binder to form a homogenous slurry by addition of few drops of 1-methyl 2-pyrollidone (NMP). The slurry was pasted onto a clean nickel foam cut into 1.0 x 1.0 cm^2 serving as current collector for three-electrode and then dried in an oven at 60 ^oC for 12 h. The capacitive performance of the electrodes was carried out with the aid of a Bio-Logic VMP300 potentiostat

(Knoxville TN 37930, USA) controlled by EC-Lab V1.40 software in a three-electrode set-up. The electrochemical measurements in three electrode configuration were carried out using glassy carbon as a counter electrode, Ag/AgCl as a reference electrode, carbon nanorods/fibers as the working electrode in 6 M KOH aqueous electrolyte. The cyclic voltammetry (CV) of the as-prepared samples were performed at different scan rates ranging from 5 to 100 mVs^{-1} within a potential window ranging from 0.0 to 0.45 V vs. Ag/AgCl. The galvanostatic charge-discharge (GCD) was performed at various specific currents ranging from 0.5 to 20 A g^{-1} in a potential window range of 0.0 V to 0.45V. The single electrode specific capacity, Q_s (mAh g^{-1}) was obtained via a GCD profiles using equation 1 below [4]:

$$Q_s = \frac{I_d \times \Delta t}{3.6} \quad (1)$$

where Q_s is the specific capacity, I_d is specific current in A g^{-1}, and Δt is time in seconds taken for a complete discharge cycle. The energy efficiency, η_E (%) was calculated from the following relations:

$$\eta_E = \frac{E_d}{E_c} \times 100\% \quad (2)$$

E_c, E_d and η_E are charge energy, discharge energy and energy efficiency from the integral of the area under the charge-discharge curve of the electrode respectively.

The columbic efficiency C_E was calculated according to the following relation [13]:

$$C_E = \frac{t_D}{t_c} \times 100\% \quad (3)$$

where t_c, t_D and C_E (%) are times for charging and discharging times with the same current, as well as the columbic efficiency respectively.

An open circuit potential of a frequency range from 10 mHz – 100 kHz was used to measure the electrochemical impedance spectroscopy (EIS) of the samples.

The two electrode asymmetric hybrid device was assembled by using the as-synthesized RGO-S nanorods/fibres as positive electrode and C-FP material as negative electrode with a thickness and diameter of 0.2 and 16 mm, respectively in a standard 2032 grade coin cell using Watman Celgard paper-based separator and 6 M KOH as electrolyte. The charge balance $Q_+ = Q_-$ was used to balance the mass of each electrode. Since the RGO-S shows a Faradic behaviour the specific capacity (Q_s) was calculated by integrating the area under the GCD curve as shown in equation (1) above. The specific capacity Q_s was then written as a function of mass, specific current and discharge time as shown below [27,28]:

$$m_+ I_{d(+)} \Delta_{t(+)} = m_- I_{d(-)} \Delta_{t(-)} \quad (4)$$

Since the same specific current was used, equation 4 can be simplified as:

$$\frac{m_+}{m_-} = \frac{\Delta_{t(-)}}{\Delta_{t(+)}} \quad (5)$$

where, m_+ and m_- are the positive and negative electrode masses respectively, $I_{d(+)}$ and $I_{d(-)}$ are positive and negative electrode specific currents respectively and $\Delta_{t(+)}$ and $\Delta_{t(-)}$ are the discharge time for the positive and negative electrode respectively.

The fabricated cell could operate in a wider potential window of 1.5 V based on the operating potential of respective electrodes that made up the device. The specific capacity, Q_s of the hybrid device was calculated following equation 1, while energy and power densities of the device with respect to the specific current were calculated according to the following equations:

$$E_d = \frac{I}{3.6*m} \int V dt \ \text{[Wh kg}^{-1}\text{]} \quad (6)$$

$$P_d = \frac{E_d}{\Delta t} \times 3600 \ [\text{W kg}^{-1}] \quad (7)$$

where, I is the applied current (mA), $\int V dt$ is the area under discharge curve of the device, m (mg) is the total mass of the active electrode, Δt is electrode discharge time in seconds, E_d and P_d are the energy and power densities, respectively, with their specified units [7,18,19,27].

3. RESULTS AND DISCUSSION

3.1. Morphological, structural and composition characterization

The surface morphology of the synthesized samples was characterized by SEM and the results are shown in Fig. 1. Reduced graphene oxide (RGO) was observed to have a sheet like structure (Fig. 1(a and b)). The sulphur doped reduced graphene oxide (RGO-S) showed a morphology, which comprises a combination of nanorods and nanofibers that is attributed to a chemical reaction that occurred between the RGO and sulphur (Fig. 1(c and d)). With an improved Hummers method, nanorods/fibres of different nanometers in length of ~150 nm were formed. It was revealed that, the technique can attain a homogenous blend of the reactants in solution whilst maintaining the reaction condition like temperature and concentration [4,29]. The improved Hummer's method as narrated in the experimental section (section 2.1) was completed by sonication and magnetic stirring, which resulted in nanorods/nanofibers formation without the use of external devices or apparatus. Throughout synthesis, the sonication and uniform stirring rate provide active sites for initiation of sulphur which act as a seed for the growth of nanorods/fibers which was not observed for RGO pristine sample. Similar morphology was obtained by Iqbal et al. and Oyedotun et al. whereby hydrothermal and refluxing method with the help of reflux set up was used to initiate the formation of nanorods [4,13]. Therefore, this study reveals that the same morphology can be obtained by addition of sulphur and constant stirring of the solution and sonication which prevents

sedimentation and force the close mixing, thus ensuring the occurrence of a homogenous reaction for the growth of nanorods/fibers like structure without hydrothermal or reflux set up. The observed SEM images in Fig. 1 (a-d) were further confirmed by the TEM micrographs in Fig. 1. (e and f) for both the RGO and RGO-S samples, respectively.

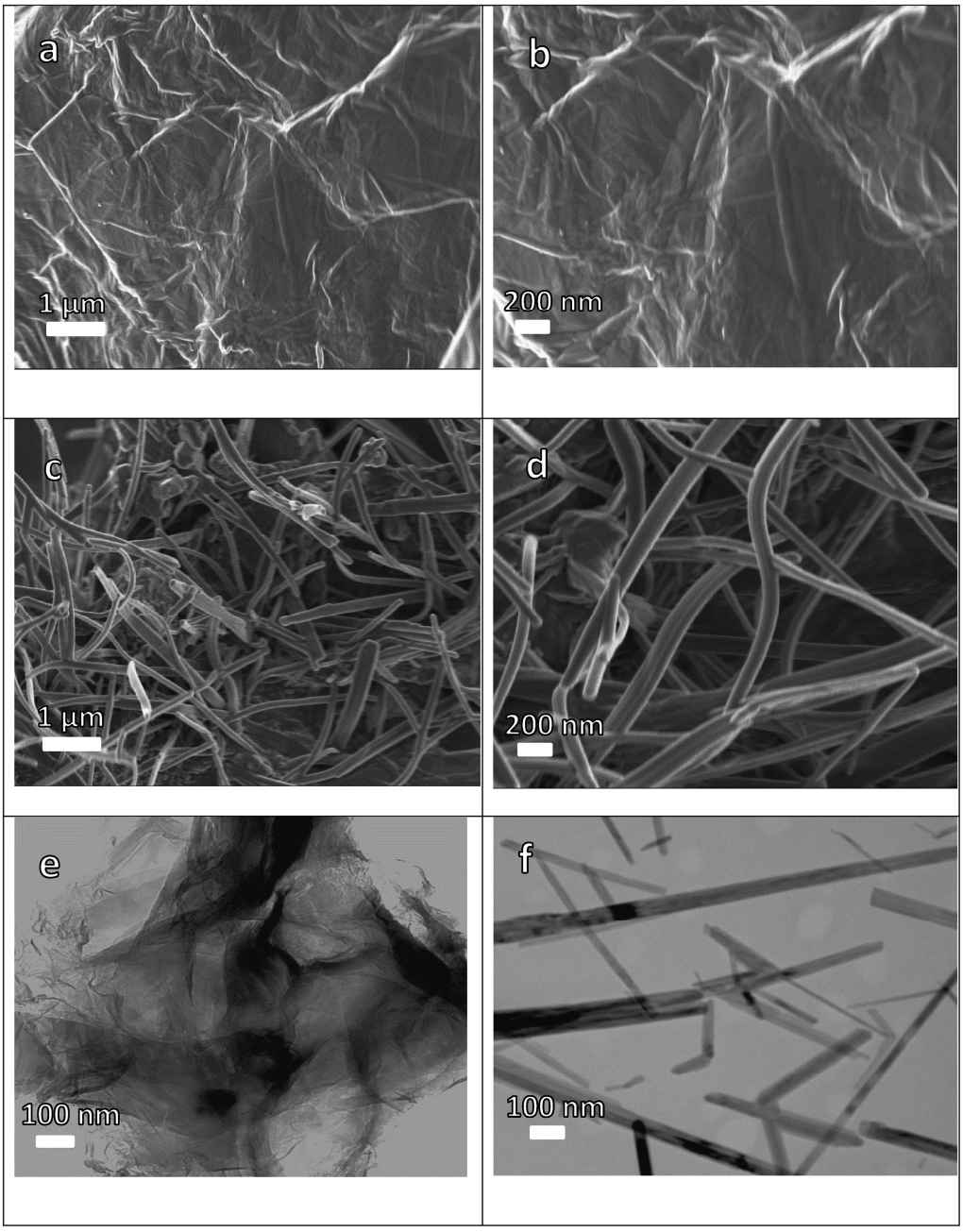

Fig. 1: (a, b) SEM images of RGO and (c, d) RGO-S at low and high magnifications, respectively, (e, f) TEM images of RGO and RGO-S, respectively.

The phase-structure analysis of the as-synthesized samples was investigated by adopting XRD according to the matching card no. JCPDS N34-0941 [30]. Fig. 2 (a) represents the XRD spectra measured within the angular range $2\theta = 5^{o} - 90^{o}$, showing a crystalline structure for both samples. The appeared diffraction peaks at around 2θ = 11.4 ^{o}C, 15.3 ^{o}C, 23 ^{o}C and 31.1 ^{o}C are due to sulphur doping, while the rest of the peaks belong to RGO. The broadness of some peaks such as 25.8 ^{o}C and 42.7 ^{o}C may be caused by the formation of defects arising from the heteroatom doping [9].

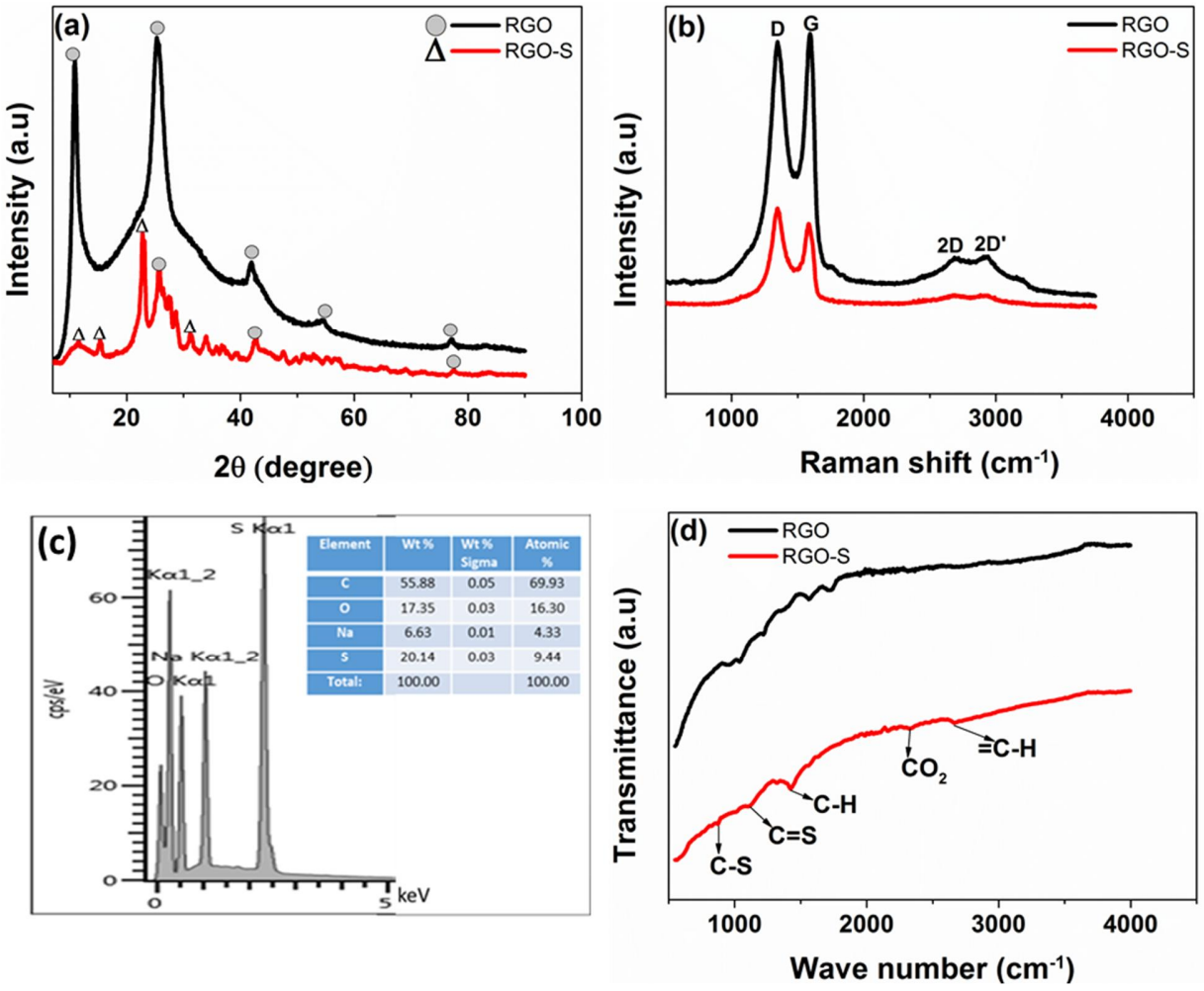

Fig. 2: (a) XRD pattern with a matching card no. JCPDS N34-0941, (b) Raman spectrum, (c) EDX spectrum and (d) FTIR spectrum of RGO and RGO-S samples, respectively.

Fig. 2(b) shows the Raman spectra of the materials, revealing four major distinct peaks at 1344 cm^{-1}, 1586 cm^{-1}, 2699 cm^{-1} and 2930 cm^{-1} corresponding to D, G, 2D and 2D' bands, respectively. The appearance of D bands corresponds to A_{1g} lattice distortion mode. The G band was due to vibrational mode in the plane E_{2g} of the sp^2 hybridized carbon [31]. 2D and 2D' is a second-order two-phonon process that displays a strong frequency dependence on the excitation laser energy. This is due to double resonance transition resulting from generation of two opposite phonon momentum which indicates the number of layers in the graphene structure [32]. The degree of defects evaluated by intensity ratio of D and G band peaks (I_d/I_g) was estimated to be 0.97 and 1.1 for RGO and RGO-S, respectively. The former displayed low value owing to the reduction in the number of defects and functional groups while the latter indicated higher value which shows that sulphur doped atom create defects in the graphene sheet due to the larger atomic size of sulphur than carbon [15,33].

Fig. 2(c) represents the EDX spectrum for sulphur-doped reduced graphene oxide sample. It was observed that the synthesized sample contains C, S and O as the major elements confirming the successful incorporation of sulphur into the matrix of RGO material. The inset to Fig. 2(c) shows EDX spectrum and inset to the figure a description of percentage weight composition of the elements in the RGO-S material. The presence of Na in the EDX spectrum is ascribed to the use of Na_2S during synthesis of the material which shows that Na was not completely removed during cleaning.

Fig. 2(d) presents the FTIR analysis of both the RGO and RGO-S samples. The FTIR peak at C=S (1124 cm^{-1}) confirms the formation of carbon-sulphur covalent bond. The existence of characteristics bands around 823 cm^{-1} is assigned to the stretching mode of C-S bonds, showing that sulfides were successfully inserted within the graphite layers forming C-S bonds. Other stretching vibrations include 1424 cm^{-1}, 2363 cm^{-1} and 2682 cm^{-1} which correspond to C-H, CO_2 and =C-H bands, respectively [34–36].

Fig. 3 (a-d) reveals the result of XPS analysis conducted to determine the types of oxygen, carbon and sulphur bonds that are present in the as-synthesized RGO-S sample. The XPS survey scans (Fig. 3(a)) of the RGO-S reveals a complete surface elemental composition with predominant peaks of O 1s, C 1s and S 2p. The Na observed in trace for the material is due to the Na_2S salt adopted in the synthesis of the RGO-S material [37]. As shown in Fig. 3(b) the strong peaks observed for O=S (530.1 eV), C=O (531.7 eV), C-OH (533.6 eV) and O=C (535.4 eV) were assigned to O 1s [38–41]. The existence of oxide species like C-OH is thermally unstable and can be removed by intensive drying. The high resolution C 1s spectra in Fig. 3(c) shows the formation of three peaks corresponding to C=C (284.6 eV), C-S/C-H/C-O (284.9 eV) and C=O (288.3 eV) [7,39,42]. The presence of C=C and C-S bonds in the C 1s spectra reflect the reduction of graphene oxide and successful doping of sulphur atoms. According to Fig. 3(d) sulphur bonding peaks assigned to thiol S-2p3/2 (C-S-C, 163.8 eV) and S-2p1/2 (C=S, 164.9 eV) are due to spin – orbit coupling [5,43,44]. The presence of thiol 3/2 and 1/2 shows that sulphur doped atoms were directly bonded to carbon atoms and reveal the defects of graphene. Furthermore, the presence of metal sulfides X_2S (159.4 eV), S^{2-} (161.2 eV) and metal sulphate $X\text{-}SO_n$ (165.0 and 167.9 eV) are due to the oxidation of S^{2-} which occurs in graphene oxide by the reduction and substitution reaction between the functional groups present in graphene oxide and sulphur atoms in Na_2S and S during synthesis [5,9,43]. The chemical compositions values were C 52%, O 26%, S 19% and Na 3% respectively. The compositions values were in a good agreement with EDX values in Fig. 2(c).

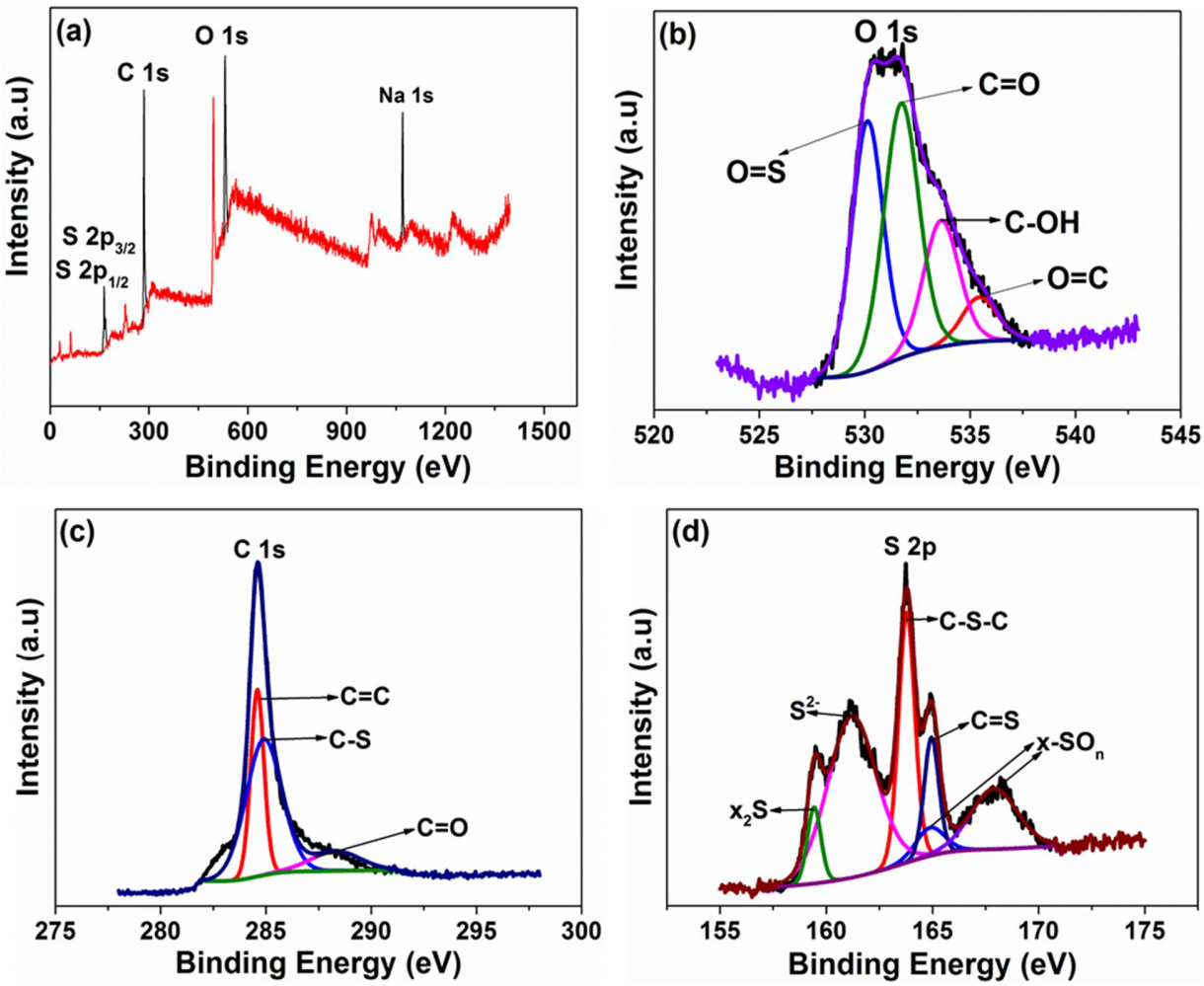

Fig. 3: (a) XPS survey spectra, core level spectrum of (b) O 1s, (c) C 1s and (d) S 1s of RGO-S of as-synthesized sample, respectively.

3.2 ELECTROCHEMICAL MEASUREMENTS

3.2.1 Three-electrode measurements

The electrochemical performance of the as-synthesized samples was first evaluated in a three-electrode system using 6 M KOH electrolyte. Fig. 4 (a, b) shows the cyclic voltammetry (CV) curves at a scan rate of 50 mVs^{-1} in both positive and negative potential windows range of -0.45 to 0.0 V and 0.0 to 0.45 V for RGO and RGO-S samples, respectively. The CV curves in the positive potential window displayed a Faradaic behavior while in the negative potential window displayed pseudocapacitive behaviour. This might be linked to the presence of functional groups

in the material and the concentration of KOH electrolyte which produces the OH^- in the positive potential window and K^+ in the negative potential window [45]. Fig. 4 (c, d) represents the galvanostatic charge/discharge (GCD) curves at a current density of 0.5 Ag^{-1} in both positive and negative potential windows for RGO and RGO-S samples, respectively. It was observed that the GCD curve is nonlinear with a potential plateau in the positive potential window and semi-linear in the negative potential window for both samples, which corresponds well with the CV curves observed in Fig. 4 (a, b). The observed oxidation peaks at 0.292 V and 0.285 V and reduction peaks at 0.180 V and 0.166 V for RGO and RGO-S, respectively in the CV curves in the positive potential window are due to the electrochemical redox reactions arising from the presence of functional groups which have high redox reactivity characteristics in the positive potential window [46]. From the results, it is observed that the current response and discharge time for the RGO-S in both the CV and GCD profiles were higher compare to that of RGO in both negative and positive operating potentials respectively. This is ascribed to addition of sulphur heteroatom into the matrix of the material [7,31] which increases electrochemical performance of RGO through increase in electrical conductivity of RGO and also plays important role in increasing capacity of RGO due to additional redox reactions. It is also clear that the positive potential window electrochemical performances are far higher than those in the negative potential window.

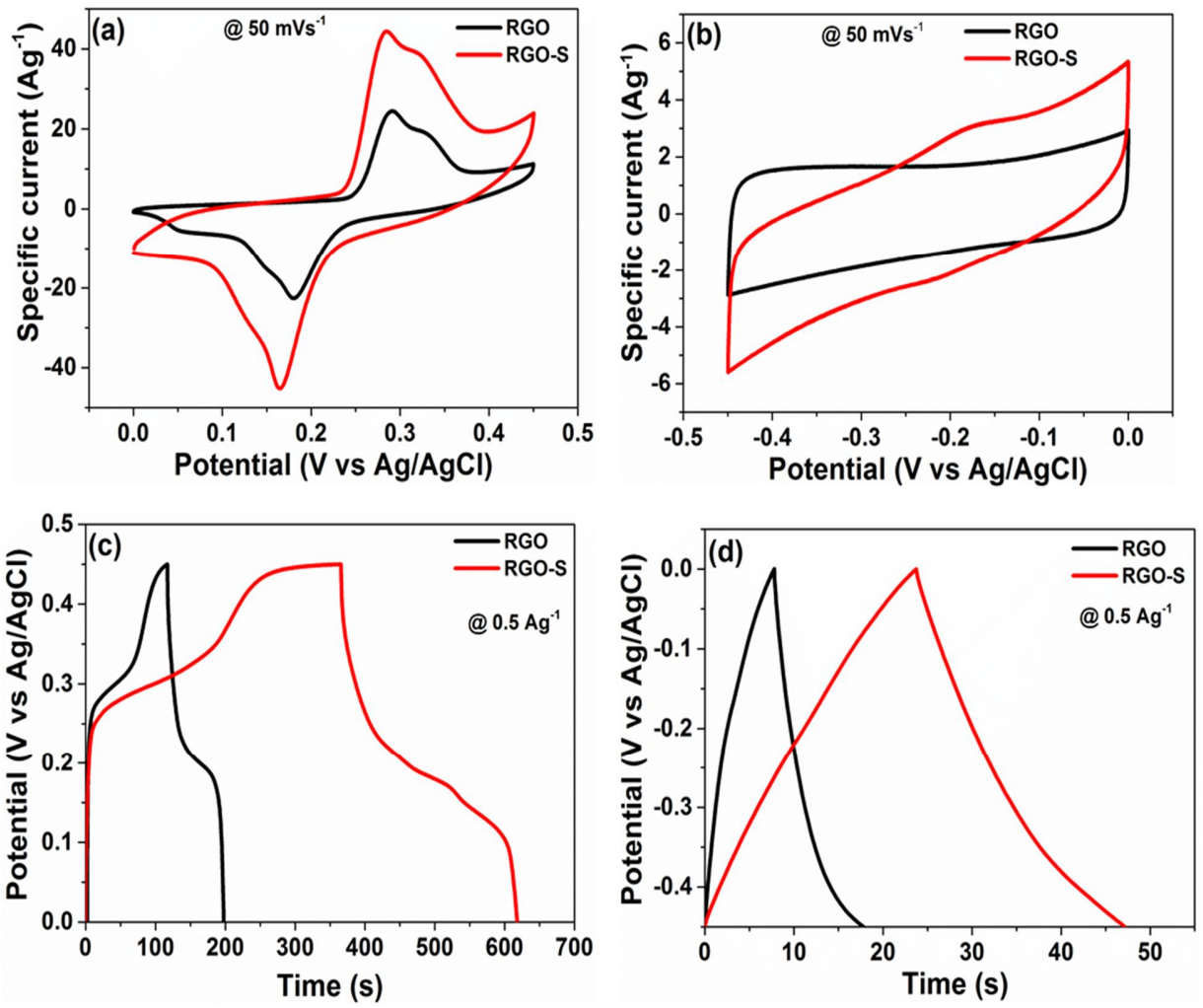

Fig. 4: (a, b) CV curves at a scan rate of 50 mVs^{-1} in both positive and negative potential windows, (c, d) GCD curves at a current density of 0.5 Ag^{-1} in both positive and negative potential windows for RGO and RGO-S sample in 6 M KOH, respectively.

Fig. 5 (a, b) reveals Columbic efficiency and energy efficiency for RGO and RGO-S electrode over a 2000 charge and discharge cycling test at 5 A g^{-1}. The half-cells could maintain 98.5 % and 98.7 % cycling stability with an energy efficiency of about 98.1 % and 98.5 % after 2000 cycles for both RGO and RGO-S respectively. It was revealed that RGO-S has high cycling stability and energy efficiency compared to RGO. This might be due to the redox reaction facilitated by sulphur doping, which enhanced the electrochemical performance and stability of the sample.

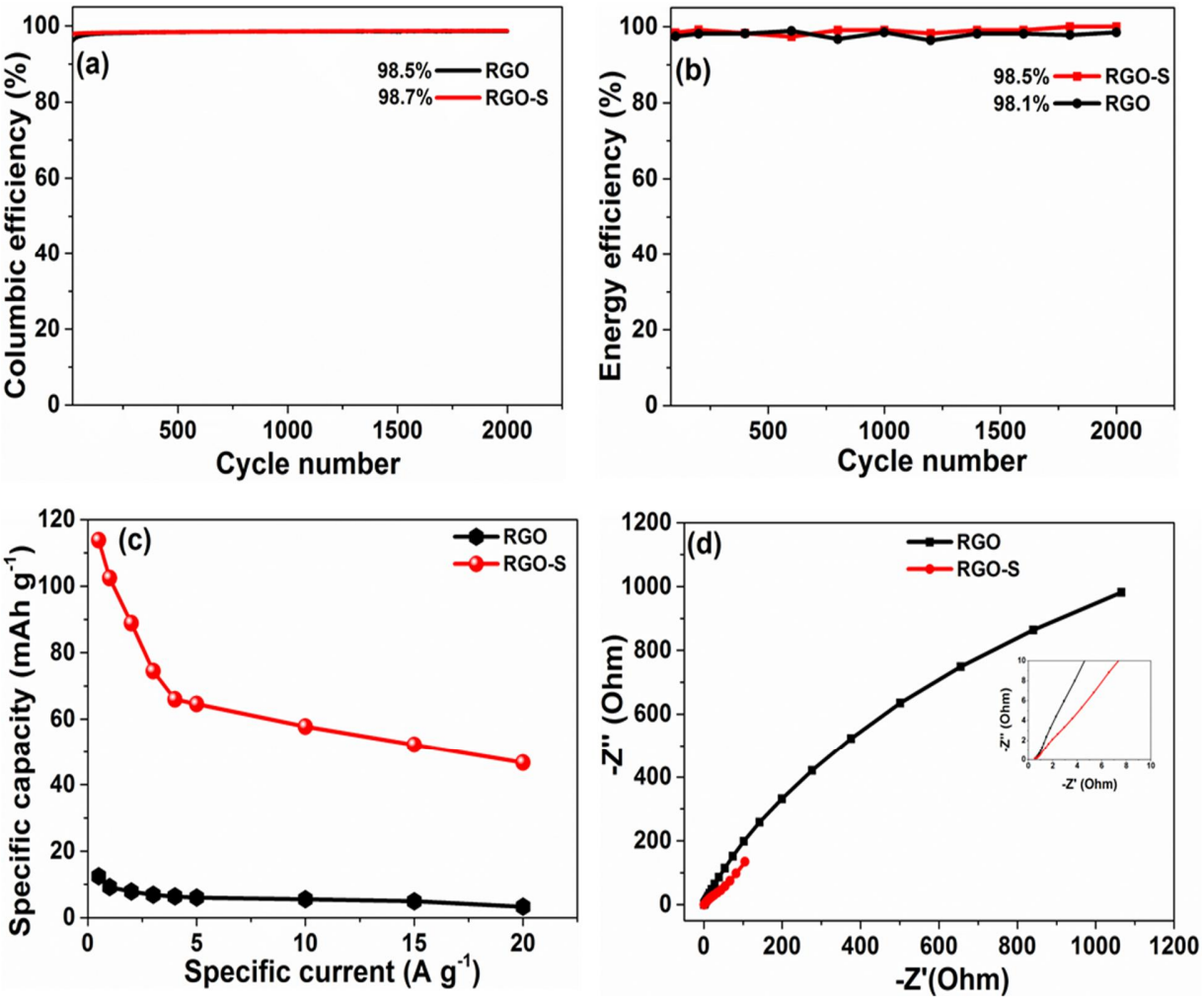

Fig. 5: (a) Cycling performance, (b) energy efficiency, (c) specific capacity against specific current and (d) EIS Nyquist plot for RGO and RGO-S sample in 6 M KOH, respectively.

Fig. 5 (c) is a representation of specific capacities against specific currents evaluated from GCD profiles using equation 1 for both RGO and RGO-S electrode materials in the positive potential window. A maximum value of 12.5 mAh g^{-1} and 113.8 mAh g^{-1} was recorded for RGO and RGO-S electrode, respectively at a specific current of 0.5 A g^{-1}. This better performance observed for the RGO-S was ascribed to the improved Hummers method adopted in the material's synthesis as well as the introduction of heteroatom (sulphur nanoparticle) into the graphene-based material, which resulted in a unique morphology, improvement in electrical conductivity and additional

redox reactions. The introduction of heteroatom can change the electronic state of graphene sheets and facilitate transportation of electrolyte's ions [3].

The EIS Nquist plots in Fig. 5(d) display characteristics frequency response of RGO and RGO-S corresponding to an AC impedance spectrum. Remarkably, low equivalent series resistance (R_S) value of about 0.43 Ω was observed for RGO-S compared to 0.65 Ω of RGO. This lower Rs value of RGO-S electrode accounts for the material's improved conductivity compared to the RGO. Also, RGO-S shows very short diffusion length compared to RGO which also indicates a great electrochemical improvement of RGO due to presence of S heteroatoms.

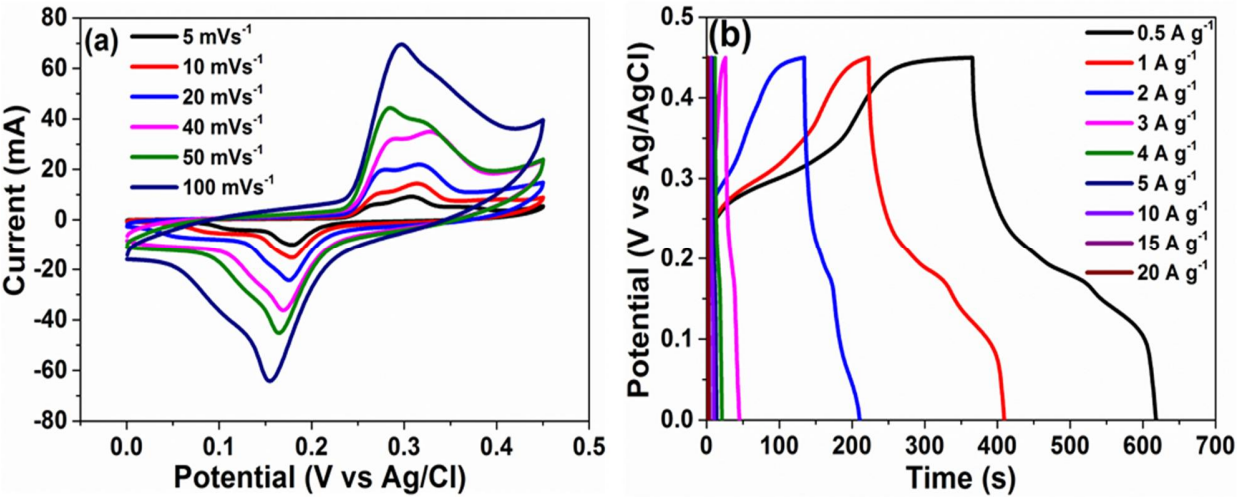

Fig. 6: (a) CV curves and (b) GCD curves of RGO-S sample in 6 M KOH, respectively.

From the above discussion, it was revealed that RGO-S performed better than RGO in terms of CV, GCD, cycling performance, energy efficiency, specific capacity and EIS Nyquist impedance. Since it was further shown that CV and GCD of RGO-S displays higher specific current and discharge time in the positive potential window than in the negative potential window, therefore, RGO-S was selected as a positive electrode material for a full cell device. Fig 6 (a) shows the CV curves of RGO-S at different scan rates ranging from 5 to 100 mV s^{-1} in a potential window range

of 0.0 – 0.45 V. Fig. 6 (b) represents the GCD curves at different specific currents from 0.5 to 20 A g^{-1}. It was observed that the GCD curves agrees well with the peaks displayed by the CV curves in Fig. 6 (a). The CV and GCD curves show the redox peaks contributed by the faradaic reaction which has resulted in enhanced specific capacity of the material as shown in Figure 5 (c).

3.2.2 Two-electrode evaluations of asymmetric RGO-S//C-FP cell

The electrochemical performance of RGO-S nanorods/fibres electrode was evaluated further in a two-electrode system. For further electrochemical analysis, an asymmetric cell designated as **RGO-S//C-FP** was assembled using RGO-S and C-FP as positive and negative electrodes respectively. Using equation (5), a mass balance ratio of 1.0:1.6 was evaluated, corresponding to a mass of 2.0 and 3.2 mg for RGO-S and C-FP electrode, respectively, resulting in a total mass of 5.2 mg/cm^2 for the asymmetric cell. The set up was completed in a standard 2032 grade coin cell sandwiched with a filter paper as the separator and 6 M KOH as electrolyte.

Fig. 7 (a) presents the CV curves of C-FP and RGO-S nanorods/fibres materials employed as negative and positive electrodes, respectively. The C-FP electrode displayed an ideal rectangular shape, indicating a reversible capacitive behavior, while the RGO-S electrode displays presence of redox peaks attributed to ongoing electrochemical oxidation and reduction reaction arising from the presence of oxygen and sulphur [3,15].

The CV curves for the asymmetric RGO-S//C-FP evaluated at different scan rates from 5 to 100 mV s^{-1} displayed a nonlinear pseudocapacitive curves as shown in Fig. 7 (b). The fabricated asymmetric cell was able to operate in a higher potential window of about 1.5 V which is a result of synergy between the positive and negative electrode materials that made up the cell. This result shows that the combination of RGO-S//C-FP improves the electrochemical performance by

facilitating the charge carriers which improve the potential window and increases the current value at the same scan rate.

Figure 7 (c) presents GCD profile of the fabricated asymmetric cell at different specific currents ranging from 0.5 to 20 A g^{-1}. The quasi linear GCD curves displayed the faradic contribution via redox reaction from RGO-S//C-FP which corresponds with the CV curves in Fig. 7 (b). This indicates that C-FP has rationalized the purely faradic behaviour of RGO-S to pseudocapacitive behaviour. This combined characteristics of faradic and EDLC is called supercapattery behavior [27,45]. Fig. 7 (d) displays the specific capacity versus specific currents of the RGO-S//C-FP cell obtained using equation (1) from GCD curves displayed in Fig. 7 (c). At a specific current of 0.5 A g^{-1}, the maximum specific capacity of about 112.7 mAh g^{-1} was recorded. Fig 7 (e) shows a capacity retention of about 85.13% for the cell and a corresponding columbic efficiency of about 99 % over 10, 000 cycles at 3 A g^{-1}, which proves an excellent long-term electrochemical stability of the asymmetric cell. Fig. 7 (f) displays the EIS before and after cycling. It was observed that an equivalent series resistance was reduced from 3 Ω to 2.5 Ω after 10, 000 cycling at 3 A g^{-1}. This could be due to wettability and also the material became more accessible to the ions after it has been exposed to a quite number of cycles [5,21].

The Ragone plot was shown in Fig. 7 (g) to compare the energy and power densities in this work and some other similar materials recently reported in the literature. From Fig. 7 (g) the energy and power densities of the fabricated cell were calculated using equations (6) and (7), respectively. Remarkably, a high energy density of 35.2 Wh kg^{-1} corresponding to a power density of 375 W kg^{-1} at a specific current of 0.5 A g^{-1} was recorded. These values were found to be in the same range and also superior to other works in the literature reporting the similar devices which have been stated in the introduction section [6,11,13,19,25].

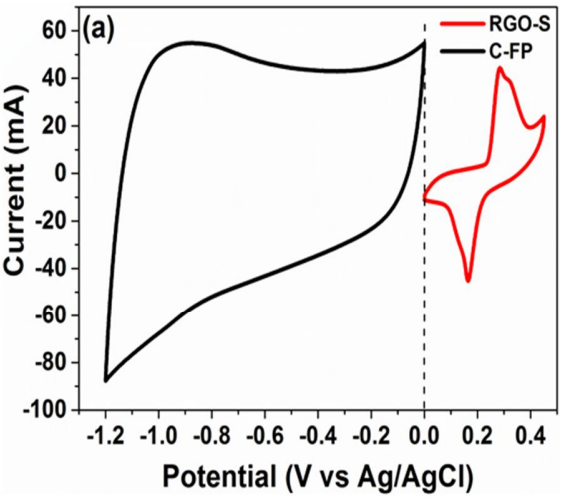
(a)
RGO-S
C-FP
Current (mA)
Potential (V vs Ag/AgCl)

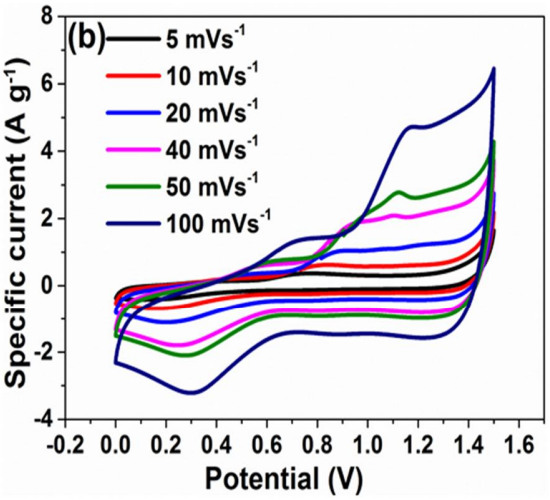
(b)
5 mVs-1
10 mVs-1
20 mVs-1
40 mVs-1
50 mVs-1
100 mVs-1
Specific current (A g-1)
Potential (V)

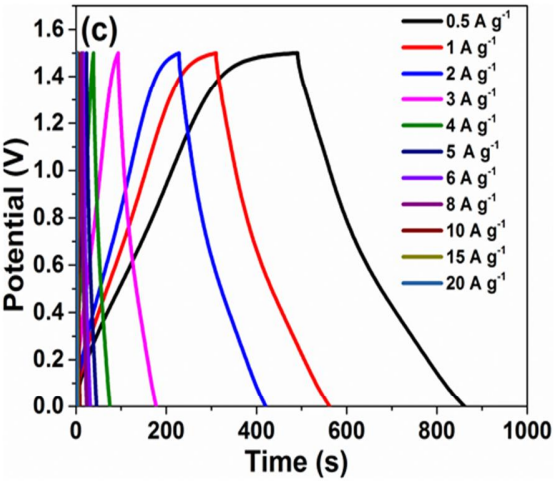
(c)
0.5 A g-1
1 A g-1
2 A g-1
3 A g-1
4 A g-1
5 A g-1
6 A g-1
8 A g-1
10 A g-1
15 A g-1
20 A g-1
Potential (V)
Time (s)

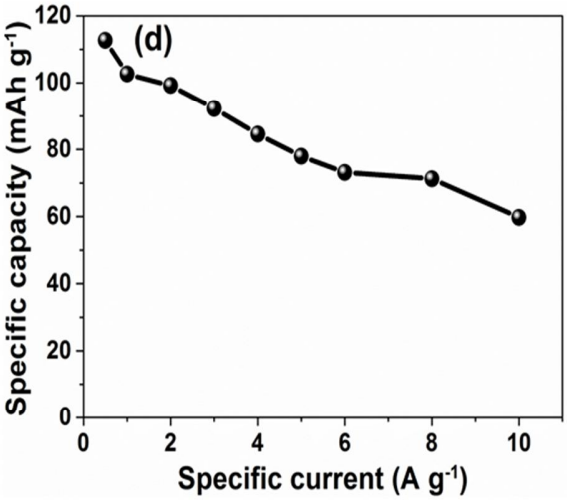
(d)
Specific capacity (mAh g-1)
Specific current (A g-1)

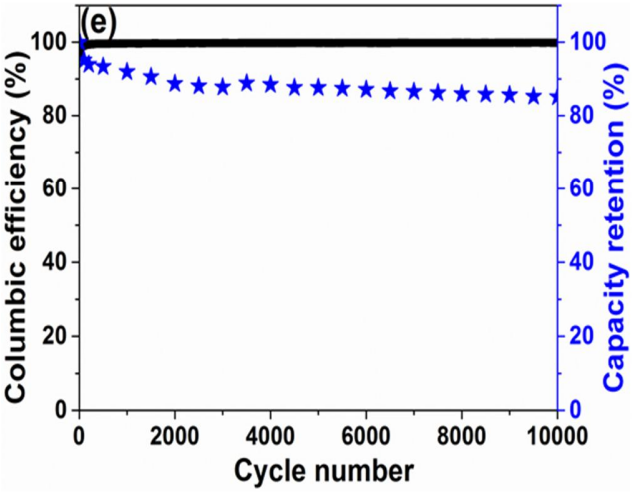
(e)
Columbic efficiency (%)
Capacity retention (%)
Cycle number

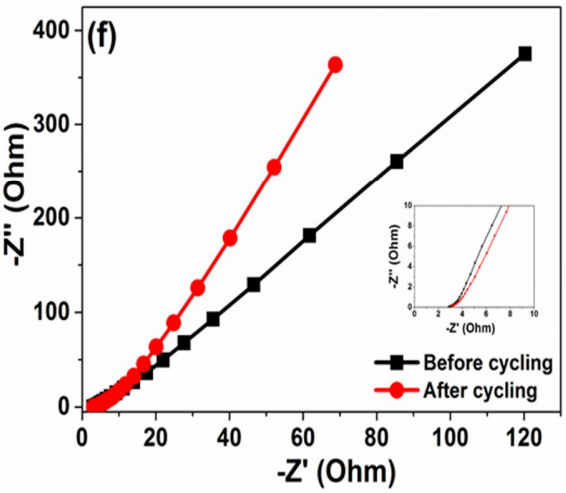
(f)
-Z'' (Ohm)
-Z' (Ohm)
Before cycling
After cycling

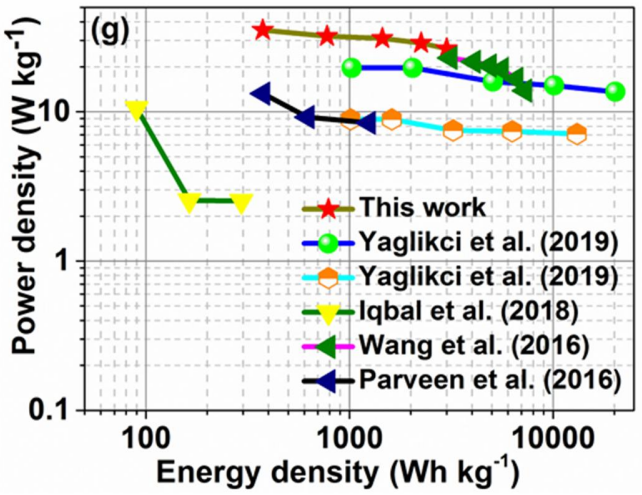

Fig. 7: (a) CV curves in both negative and positive potential windows, (b) CV curves, (c) GCD curves, (d) specific capacity versus specific current (e) cycling performance versus capacity retention, (f) EIS Nyquist plot before and after cycling and (g) Ragone plot of RGO-S //C-FP, respectively.

4. CONCLUSION

Sulphur-doped reduced graphene oxide (RGO-S) was successfully synthesized using an improved Hummers method. The characterization of the material revealed the formation of carbon nanorods/fibers material without an addition of any device or apparatus for influencing the formation/growth of nanorods/fibers like structure. This shows that sulphur was successfully incorporated into graphene oxide by the formation of C-S bond. This was further confirmed from the material's crystalline structure showing composition of S, C, O and Na. The fabricated three-electrode material displayed a highest specific capacity of 113.8 mAh g^{-1} at 0.5 A g^{-1}. The half-cell could retain a columbic efficiency of about 98.7 % with corresponding energy efficiency of about 98.5 % over 2,000 constant charge/discharge cycle at a specific current of 5 A g^{-1}. Remarkably, the fabricated hybrid device with carbonized iron cations (C-FP) and the RGO-S composite delivered a specific capacity of 112.7 mAh g^{-1} , high energy and power densities of 35.2 Wh kg^{-1} and 375 W kg^{-1} at 0.5 A g^{-1} within a 1.5 V operating potential, respectively. A good cycling stability performance with an energy efficiency of 99% was observed for the device for up to 10,000 cycling

at a specific current of 3 A g^{-1}. The fabricated sample revealed good electrochemical properties which offer the materials in question as for supercapacitor application.

ACKNOWLEDGEMENTS

This work is based on the research supported by the South African Research Chairs Initiative of the Department of Science and Technology and National Research Foundation of South Africa (Grant No. 61056). Any opinion, finding, and conclusion expressed in this material are that of the authors, and the NRF does not accept any liability in this regard. Delvina Japhet Tarimo acknowledges the financial support from NRF through SARChI chair in Carbon Technology and Materials. Patrick Urbankowski of the Department of Materials Science and Engineering, Drexel University, USA is acknowledged for performing XPS measurements.

REFERENCES

[1] Moriarty P, Honnery D. Hydrogen's role in an uncertain energy future. International Journal of Hydrogen Energy 2009;34:31–9. https://doi.org/10.1016/j.ijhydene.2008.10.060.

[2] Lin KS, Adhikari AK, Ku CN, Chiang CL, Kuo H. Synthesis and characterization of porous HKUST-1 metal organic frameworks for hydrogen storage. International Journal of Hydrogen Energy 2012;37:13865–71. https://doi.org/10.1016/j.ijhydene.2012.04.105.

[3] Yu X, Park HS. Sulfur-incorporated, porous graphene films for high performance flexible electrochemical capacitors. Carbon 2014;77:59–65. https://doi.org/10.1016/j.carbon.2014.05.002.

[4] Oyedotun KO, Madito MJ, Bello A, Momodu DY, Mirghni AA, Manyala N. Investigation of graphene oxide nanogel and carbon nanorods as electrode for electrochemical supercapacitor. Electrochimica Acta 2017;245:268–78.

https://doi.org/10.1016/j.electacta.2017.05.150.

[5] Yu X, Kang Y, Park HS. Sulfur and phosphorus co-doping of hierarchically porous graphene aerogels for enhancing supercapacitor performance. Carbon 2016;101:49–56. https://doi.org/10.1016/j.carbon.2016.01.073.

[6] Yaglikci S, Gokce Y, Yagmur E, Aktas Z. The performance of sulphur doped activated carbon supercapacitors prepared from waste tea. Environmental Technology 2019;0:1–13. https://doi.org/10.1080/09593330.2019.1575480.

[7] Duraivel M, Nagappan S, Balamuralitharan B, Selvam S, Karthick SN, Prabakar K, et al. Superior one-pot synthesis of a doped graphene oxide electrode for a high power density supercapacitor. New Journal of Chemistry 2018;42:11093–101. https://doi.org/10.1039/c8nj01672k.

[8] Karthik N, Edison TNJI, Atchudan R, Xiong D, Lee YR. Electro-synthesis of sulfur doped nickel cobalt layered double hydroxide for electrocatalytic hydrogen evolution reaction and supercapacitor applications. Journal of Electroanalytical Chemistry 2019;833:105–12. https://doi.org/10.1016/j.jelechem.2018.11.028.

[9] Zhang X, Yan P, Zhang R, Liu K, Liu Y, Liu T, et al. A novel approach of binary doping sulfur and nitrogen into graphene layers for enhancing electrochemical performances of supercapacitors. Journal of Materials Chemistry A 2016;4:19053–9. https://doi.org/10.1039/c6ta08482f.

[10] Zhu J, Zhou W, Zhou Y, Cheng X, Yang J. Cobalt Sulfide/Reduced Graphene Oxide Nanocomposite with Enhanced Performance for Supercapacitors. Journal of Electronic Materials 2019;48:1531–9. https://doi.org/10.1007/s11664-018-06910-z.

[11] Li Y, Wang G, Wei T, Fan Z, Yan P. Nitrogen and sulfur co-doped porous carbon nanosheets derived from willow catkin for supercapacitors. Nano Energy 2016;19:165–75. https://doi.org/10.1016/j.nanoen.2015.10.038.

[12] Chen Q, Cai D, Zhan H. Construction of reduced graphene oxide nanofibers and cobalt sulfide nanocomposite for pseudocapacitors with enhanced performance. Journal of Alloys and Compounds 2017;706:126–32. https://doi.org/10.1016/j.jallcom.2017.02.189.

[13] Iqbal MF, Ashiq MN, Razaq A, Saleem M, Parveen B, Hassan MU. Excellent

electrochemical performance of graphene oxide based strontium sulfide nanorods for supercapacitor applications. Electrochimica Acta 2018;273:136–44. https://doi.org/10.1016/j.electacta.2018.04.014.

[14] Yang J, Gunasekaran S. Electrochemically reduced graphene oxide sheets for use in high performance supercapacitors. Carbon 2013;51:36–44. https://doi.org/10.1016/j.carbon.2012.08.003.

[15] Yu X, Park SK, Yeon SH, Park HS. Three-dimensional, sulfur-incorporated graphene aerogels for the enhanced performances of pseudocapacitive electrodes. Journal of Power Sources 2015;278:484–9. https://doi.org/10.1016/j.jpowsour.2014.12.102.

[16] Snook GA, Kao P, Best AS. Conducting-polymer-based supercapacitor devices and electrodes. Journal of Power Sources 2011;196:1–12. https://doi.org/10.1016/j.jpowsour.2010.06.084.

[17] Barik R, Devi N, Perla VK, Ghosh SK, Mallick K. Stannous sulfide nanoparticles for supercapacitor application. Applied Surface Science 2019;472:112–7. https://doi.org/10.1016/j.apsusc.2018.03.172.

[18] Yang Y, Liu L, Tang Y, Zhang Y, Jia D, Kong L. Bamboo-like carbon nanotubes containing sulfur for high performance supercapacitors. Electrochimica Acta 2016;191:846–53. https://doi.org/10.1016/j.electacta.2016.01.149.

[19] Parveen N, Ansari MO, Ansari SA, Cho MH. Simultaneous sulfur doping and exfoliation of graphene from graphite using an electrochemical method for supercapacitor electrode materials. Journal of Materials Chemistry A 2015;4:233–40. https://doi.org/10.1039/c5ta07963b.

[20] Elmouwahidi A, Castelo-Quibén J, Vivo-Vilches JF, Pérez-Cadenas AF, Maldonado-Hódar FJ, Carrasco-Marín F. Activated carbons from agricultural waste solvothermally doped with sulphur as electrodes for supercapacitors. Chemical Engineering Journal 2018;334:1835–41. https://doi.org/10.1016/j.cej.2017.11.141.

[21] Han J, Zhang LL, Lee S, Oh J, Lee KS, Potts JR, et al. Generation of B-doped graphene nanoplatelets using a solution process and their supercapacitor applications. ACS Nano 2013;7:19–26. https://doi.org/10.1021/nn3034309.

[22] Khandelwal M, Li Y, Molla A, Hyun Hur S, Suk Chung J. Single precursor mediated one-step synthesis of ternary-doped and functionalized reduced graphene oxide by pH tuning for energy storage applications. Chemical Engineering Journal 2017;330:965–78. https://doi.org/10.1016/j.cej.2017.08.040.

[23] Kurmaev EZ, Galakhov A V., Moewes A, Moehlecke S, Kopelevich Y. Interlayer conduction band states in graphite-sulfur composites. Physical Review B - Condensed Matter and Materials Physics 2002;66:1–3. https://doi.org/10.1103/PhysRevB.66.193402.

[24] Zhang J, Yang Z, Wang X, Ren T, Qiao Q. Homogeneous sulphur-doped composites: Porous carbon materials with unique hierarchical porous nanostructure for super-capacitor application. RSC Advances 2016;6:84847–53. https://doi.org/10.1039/c6ra17231h.

[25] Parveen N, Ansari MO, Ansari SA, Cho MH. Erratum: Simultaneous sulfur doping and exfoliation of graphene from graphite using an electrochemical method for supercapacitor electrode materials (Journal of Materials Chemistry A (2016) 4 (233-240)). Journal of Materials Chemistry A 2016;4:12668–9. https://doi.org/10.1039/C6TA90155G.

[26] Kannappan S, Kaliyappan K, Manian RK, Pandian AS, Yang H, Lee YS, et al. Graphene based Supercapacitors with Improved Specific Capacitance and Fast Charging Time at High Current Density 2013.

[27] Oyedotun KO, Madito MJ, Momodu DY, Mirghni AA, Masikhwa TM, Manyala N. Synthesis of ternary NiCo-MnO2 nanocomposite and its application as a novel high energy supercapattery device. Chemical Engineering Journal 2018;335:416–33. https://doi.org/10.1016/j.cej.2017.10.169.

[28] Mirghni AA, Oyedotun KO, Mahmoud BA, Bello A, Ray SC, Manyala N. Nickel-cobalt phosphate/graphene foam as enhanced electrode for hybrid supercapacitor. Composites Part B: Engineering 2019;174:106953. https://doi.org/10.1016/j.compositesb.2019.106953.

[29] Tang Y, Zhang Y, Deng J, Wei J, Tam H Le, Chandran BK, et al. Mechanical force-driven growth of elongated be[1] Y. Tang, Y. Zhang, J. Deng, J. Wei, H. Le Tam, B.K. Chandran, et al., Mechanical force-driven growth of elongated bending Tio 2 -based nanotubular materials for ultrafast rechargeable lithium ion batteries. Advanced Materials 2014;26:6111–8. https://doi.org/10.1002/adma.201402000.

[30] Guo Y, Zhao J, Yang S, Yu K, Wang Z, Zhang H. Preparation and characterization of monoclinic sulfur nanoparticles by water-in-oil microemulsions technique. Powder Technology 2006;162:83–6. https://doi.org/10.1016/j.powtec.2005.12.012.

[31] Yu X, Park HS. Sulfur-incorporated, porous graphene films for high performance flexible electrochemical capacitors. Carbon 2014. https://doi.org/10.1016/j.carbon.2014.05.002.

[32] Escobar-Alarcón L, Espinosa-Pesqueira ME, Solis-Casados DA, Gonzalo J, Solis J, Martinez-Orts M, et al. Two-dimensional carbon nanostructures obtained by laser ablation in liquid: effect of an ultrasonic field. Applied Physics A: Materials Science and Processing 2018;124:1–7. https://doi.org/10.1007/s00339-018-1559-8.

[33] Zhang J, Jiang M, Xing L, Qin K, Liu T, Zhou J, et al. Three Dimensional Sulfur-doped Graphene Hydrogels with Tetrathiafulvalene for High Performance Supercapacitors. Chinese Journal of Chemistry 2016;34:46–52. https://doi.org/10.1002/cjoc.201500656.

[34] Ouyang Z, Lei Y, Chen Y, Zhang Z, Jiang Z, Hu J, et al. Preparation and Specific Capacitance Properties of Sulfur, Nitrogen Co-Doped Graphene Quantum Dots. Nanoscale Research Letters 2019;14:219. https://doi.org/10.1186/s11671-019-3045-4.

[35] Qu D, Zheng M, Du P, Zhou Y, Zhang L, Li D, et al. Highly luminescent S, N co-doped graphene quantum dots with broad visible absorption bands for visible light photocatalysts. Nanoscale 2013;5:12272–7. https://doi.org/10.1039/c3nr04402e.

[36] Compounds O. Rao, C. N. R., R. Venkataraghavan, and T. R. Kasturi. “Contribution to the infrared spectra of organosulphur compounds.” Canadian journal of chemistry 42.1 (1964): 36-42. Science 1964;42:36–42.

[37] Oyedotun KO, Masikhwa TM, Lindberg S, Matic A, Johansson P, Manyala N. Comparison of ionic liquid electrolyte to aqueous electrolytes on carbon nanofibres supercapacitor electrode derived from oxygen-functionalized graphene. Chemical Engineering Journal 2019;375:121906. https://doi.org/10.1016/j.cej.2019.121906.

[38] Longo A, Verucchi R, Aversa L, Tatti R, Ambrosio A, Orabona E, et al. Graphene oxide prepared by graphene nanoplatelets and reduced by laser treatment. Nanotechnology 2017;28:224002. https://doi.org/10.1088/1361-6528/aa6c3c.

[39] Lin W, Chen Y, Li P, He J, Zhao Y, Wang Z, et al. Enhanced Performance of Lithium

Sulfur Battery with a Reduced Graphene Oxide Coating Separator. Journal of The Electrochemical Society 2015;162:A1624–9. https://doi.org/10.1149/2.0891508jes.

[40] Drewniak S, Muzyka R, Stolarczyk A, Pustelny T, Kotyczka-Morańska M, Setkiewicz M. Studies of reduced graphene oxide and graphite oxide in the aspect of their possible application in gas sensors. Sensors (Switzerland) 2016;16. https://doi.org/10.3390/s16010103.

[41] Song X, Chen Q, Shen E, Liu H. Supercapacitive performances of few-layer MoS 2 on reduced graphene oxides 2019:911–23.

[42] Chu RX, Lin J, Wu CQ, Zheng J, Chen YL, Zhang J, et al. Reduced graphene oxide coated porous carbon-sulfur nanofiber as a flexible paper electrode for lithium-sulfur batteries. Nanoscale 2017;9:9129–38. https://doi.org/10.1039/c7nr02423a.

[43] Wang X, Gao T, Han F, Ma Z, Zhang Z, Li J, et al. Stabilizing high sulfur loading Li–S batteries by chemisorption of polysulfide on three-dimensional current collector. Nano Energy 2016;30:700–8. https://doi.org/10.1016/j.nanoen.2016.10.049.

[44] Chen L, Cui X, Wang Y, Wang M, Qiu R, Shu Z, et al. One-step synthesis of sulfur doped graphene foam for oxygen reduction reactions 2014:3420–3. https://doi.org/10.1039/c3dt52253a.

[45] Rantho MN, Madito MJ, Manyala N. Symmetric supercapacitor with supercapattery behavior based on carbonized iron cations adsorbed onto polyaniline. Electrochimica Acta 2018;262:82–96. https://doi.org/10.1016/j.electacta.2018.01.001.

[46] Conway BE, Ku JCH, Ho FC. The electrochemical surface reactivity of iron sulfide, FeS2. Journal of Colloid And Interface Science 1980;75:357–72. https://doi.org/10.1016/0021-9797(80)90461-0.